Intense Isolated Ultrashort Attosecond Pulse Generation in a Multi-Cycle Three-Colour Laser Field

Gang-Tai Zhang

Department of Physics and Information Technology, Baoji University of Arts and Sciences, Baoji 721016, China

Reprint requests to G.-T. Z; E-mail: gtzhang79@163.com

Z. Naturforsch. **69a**, 673 – 686 (2014) / DOI: 10.5560/ZNA.2014-0067
Received May 28, 2014 / revised August 17, 2014 / published online November 20, 2014

An efficient method for generating an intense isolated ultrashort attosecond pulse is presented theoretically. By adding a 267 nm controlling pulse to a multi-cycle two-colour field, not only the spectral cutoff and the yields of the harmonic spectrum are evidently enhanced, but also the selection of the single quantum path is realised. Then a high-efficiency supercontinuum with a 504 eV bandwidth and smooth structure is obtained, which enables the production of an intense isolated 30 as pulse. In addition, the influences of the laser parameters on the supercontinuum and isolated attosecond pulse are investigated.

Key words: High-Order Harmonic Generation; Isolated Attosecond Pulse; Quantum Path Selection; Three-Colour Field.

1. Introduction

The appearance and development of attosecond pulses has opened up a new field of time-resolved studies with high precision [1, 2], which provides an important tool for detecting and controlling the electron dynamics inside atoms and molecules with unprecedented resolutions [3, 4]. So far, high-order harmonic generation (HHG) offers a unique way to produce attosecond pulses in experiments. The HHG process can be well depicted by the classical three-step model [5]: ionization, acceleration, and recombination. In detail, an electron first tunnels through the barrier formed by the atomic potential and the laser field, then it oscillates almost freely in the laser field, and finally it may return to the ground state by recombining with the parent ion and emit radiation. According to the model, the maximum harmonic photon energy is equal to $I_p + 3.17U_p$, where I_p is the atomic ionization potential, and U_p is the ponderomotive energy of the electron in the laser field. For a long laser pulse, this process is repeated every half-cycle of the driving field, which results in an attosecond pulse train (APT) with a periodicity of one-half of an optical cycle. The underlying physics behind this phenomenon is that each harmonic is mainly associated to the contribution of two electron paths (so-called long and short paths) within each half optical cycle [5]. Since these two electron paths have very different emission times, the harmonics are not locked in phase. As a result, the superposition of several harmonics leads to an irregular APT including at least two bursts per half optical cycle of the driving field [6].

For practical application, since an isolated attosecond pulse is preferable to an APT, how to produce an isolated attosecond pulse has attracted a lot of attention [7, 8]. Currently, there are two methods to create such an isolated attosecond pulse. One is HHG from a few-cycle driving pulse, the other is HHG from the temporal confined pulse by polarization gating. With the first method, an isolated 80 as pulse has been realised by a 3.3 fs/720 nm carrier-envelope phase stabilized laser field [9]. With the second method, a single 130 as extreme-ultraviolet (XUV) pulse has been demonstrated experimentally [10]. Moreover, ionization gating [11], chirped pulse [12], double optical gating (DOG) [13, 14], generalized DOG (GDOG) [15], and multi-cycle laser sources [16, 17] have been proposed for producing desirable isolated attosecond pulses. Very recently, Zhao et al. [18] have produced a 67 as pulse with a 7 fs/750 nm laser pulse, which is the known shortest attosecond pulse at present. By using these techniques mentioned above, scientists can generate a regular single attosecond pulse by filtering several consecutive harmonics in the cutoff or plateau

region. However, the bandwidth of the XUV supercontinuum is narrow and the spectral efficiency is low, thus the application of the generated attosecond pulse is limited. To broaden the bandwidth of the generated attosecond pulse or enhance the XUV emission yield, some methods had been proposed. It has been proposed that the two-colour control scheme can significantly broaden the bandwidth of the attosecond pulse [19 – 21], and then an isolated sub-100 as pulse can be achieved. In two-colour scheme, the supercontinuum always originates from the electron ionized in that half cycle with the second strongest electric peak of the driving pulse. This intrinsic dynamic property leads to a two-plateau structure in the harmonic spectrum, and the generated supercontinuum locates in the second plateau with much lower efficiency. To improve the intensity of the attosecond pulse, the harmonic efficiency of the supercontinuum region should be enhanced. One of the most important methods of enhancing the harmonic efficiency is to prepare the initial state as a coherent superposition of two bound states, which was first proposed by Gauthey et al. [22]. Evident advantages of using coherent superposition state to obtain high conversion efficiency have been proved by Wang et al. [23]. The root cause lies in that it can induce dipole transitions between the continuum and the ground state via the excited state responsible for the ionization. In addition, this approach also has the potential to generate a high-efficiency supercontinuum with single quantum path, which results in the production of intense isolated short attosecond pulse, such as intense 45 as pulse using two-colour field in combination with a coherent superposition state [24], intense 38 as isolated pulse from a coherent superposition state by quantum path control in a multi-cycle two-colour field [25], intense isolated 150 as pulse generation with a few-cycle driving pulse in the pre-excited medium [26], intense isolated 34 as pulse with the coherent superposition initial state in the two-colour chirped pulse [27], efficient isolated attosecond pulse emission from a pre-excited medium driven by local nanoplasmonic fields [28]. In our previous work [29], by the combination of the single chirped pulse and the coherent superposition state, we obtained a high-efficient broadband supercontinuum with single quantum path contribution, and then an intense isolated 23 as pulse is generated directly. Another alternative way for enhancing the harmonic efficiency is to use an attosecond ionization control scheme, which can control electron dynamics to produce an efficient single attosecond pulse. For example, Zhao et al. [30] demonstrated that the enhancement of the HHG plateau near the cutoff and the generation of an intense isolated 57 as pulse can be achieved by using an intense few-cycle shaped laser and an ultraviolett (UV) attosecond pulse. Lan et al. [11] showed that the efficient generation of an isolated 130 as pulse is obtained using a few-cycle infrared (IR) driving pulse in combination with a UV attosecond controlling pulse. Moreover, they also showed that an efficient supercontinuum can be generated by UV-assisted midinfrared (MIR) plasmonic fields, then a strong isolated attosecond pulse can be directly filtered out from the UV-assisted harmonic spectrum and its efficiency is about five orders higher than that in the MIR driving alone [31]. By properly adding a high-order harmonic pulse to the two-colour field, Feng and Chu [32] not only realised the intensity enhancement of HHG from the He^+ ion or He atom but also obtained an intense isolated attosecond pulse as short as 41 as (He^+) and 46 as (He).

Moreover, control of quantum paths is another fascinating way to produce an isolated broadband ultrashort pulse. In the single-atom response, the quantum path control can be realised by using a two-colour field [21, 33] or an APT [34, 35]. For the real scenario, a full description of HHG requires not only the laser–atom interaction at the microscopic level but also the propagation of driving field and high harmonics through the gas medium at the macroscopic level. In particular, the phase matching in the propagation plays an important role in the HHG [36, 37]. By carefully adjusting the gas pressure or the position of the laser focus, the phase matching conditions for either a short quantum path or a long one are realised, and then a single quantum path can be macroscopically selected [38, 39]. Gaarde et al. [40] reviewed the macroscopic aspects of attosecond pulse production in a number of different generation schemes and showed that macroscopic effects such as phase matching and ionization always play a role in this selection process, in most cases enabling the formation of the attosecond pulses and in a few cases limiting it.

HHG with multi-colour field schemes has been extensively investigated [41 – 52]. It has been shown that this method can generate energetic harmonic photons [41 – 44] and effectively control the electronic dynamics in the HHG process to produce a single ultrashort attosecond pulse [45 – 52]. However, most of

the driving pulses in these three-colour schemes are limited to a few-cycle regime, which are not easy to achieve in a general laboratory. In this work, based on the simulation of the single-atom response, we numerically investigate the HHG and isolated attosecond pulse generation from one-dimensional (1D) model He^+ ion driven by a multi-cycle three-colour field. Our aim is to explore the possibilities of both extending the spectral cutoff and enhancing the harmonic efficiency to produce an intense isolated ultrashort attosecond pulse. The numerical calculations show that this method can not only extend the harmonic cutoff and generate an ultrabroad supercontinuum, but also enhance the harmonic yields of the generated spectrum. As a result, a high-efficient supercontinuum with a 504 eV bandwidth is achieved. Since the supercontinuum mainly originates from the contribution of the single short path, an intense isolated 30 as pulse is directly obtained. Additionally, the influences of the laser parameters including the time delay and laser intensity on the supercontinuum and isolated 30 as pulse generation are also investigated. To better understand the physical origin of the HHG process, we perform the classical trajectory simulation and quantum time–frequency analysis and also calculate the time-dependent ionization probability and the ionization rate by the Ammosov–Delone–Krainov (ADK) model.

2. Theoretical Model and Method

The HHG and attosecond pulse generation can be investigated by solving the 1D time-dependent Schrödinger equation within the single-active electron approximation. In the dipole approximation, it is given by (atomic units are used)

$$\mathrm{i}\frac{\partial}{\partial t}\psi(x,t) = \left[-\frac{1}{2}\frac{\partial^2}{\partial x^2} + V(x) - xE(t)\right]\psi(x,t), \quad (1)$$

where $V(x) = -z\Big/\sqrt{x^2+a}$ is the soft Coulomb potential. The parameters z and a are adopted to be 2 and 0.5 to match the ionization energy of 54.4 eV for the ground state of the helium ion (He^+). The time-varying electric field $E(t)$ is chosen as the superposition of a two-colour field (800 nm and 1600 nm) and a 267 nm controlling pulse, which is expressed by

$$E(t) = E_1 f_1(t)\cos(\omega_1 t + \phi_1) + E_2 f_2(t)\cos(\omega_2 t + \phi_2) + E_3 f_3(t+\tau_{\mathrm{delay}})\cos[\omega_3(t+\tau_{\mathrm{delay}}) + \phi_3]. \quad (2)$$

Here, E_i and ω_i ($i = 1-3$) are the peak amplitudes and frequencies of the electric fields of the 800 nm fundamental, 1600 nm subharmonic, and 267 nm controlling pulses, respectively. ϕ_i ($i = 1-3$) are the corresponding carrier-envelope phases (CEPs) and are set as 0. This is because our calculations show that varying the three fields' CEPs does not generate a much better harmonic spectrum. $f_i(t) = \exp[-4\ln 2(t/\tau_i)^2]$ ($i = 1-3$) present the envelopes of the three pulses, and τ_i ($i = 1-3$) are the corresponding pulse duration at full-width of half-maximum. We have changed the pulse durations of these three laser pulses, and found that the spectral profile and the harmonic efficiency as well as the isolated attosecond pulse generation are little affected when the pulse durations of the 1600 nm and 267 nm laser pulses are changed from 10 fs to 24 fs, whereas the duration of the 800 nm fundamental pulse should be controlled within 10 fs. Therefore, for simplicity, we shall take $\tau_1 = \tau_3 = 10$ fs and $\tau_2 = 24$ fs throughout this paper. $\tau_{\mathrm{delay}} = 0.28\,T_1$ (T_1 is the optical cycle of the 800 nm driving pulse) is the time delay of the 267 nm controlling pulse with respect to the fundamental pulse. Note that the time delay is not restricted to $0.28\,T_1$; this will be clarified later on. In our simulation, we choose the intensities of the three laser pulses as $2\cdot10^{15}$ W/cm^2, $2\cdot10^{14}$ W/cm^2, and $3\cdot10^{14}$ W/cm^2, respectively.

Equation (1) can be solved numerically by means of the split-operator method [53], where the length of the integration grid is 2457.6, the spatial step is 0.15, and the time step is 0.05. A $\cos^{1/8}$ mask function that varies from 1 to 0 over a relatively narrow range is introduced after each time evolution step to prevent reflection of the wavefunction from the boundary. After the time-dependent wave function $\psi(x,t)$ is determined, the time-dependent dipole acceleration $d(t)$ is calculated by Ehrenfest's theorem [54]:

$$d(t) = \langle\psi(x,t)|-\frac{\partial V(x)}{\partial x} + E(t)\,|\psi(x,t)\rangle. \quad (3)$$

The harmonic spectrum P_A ($q\omega_1$) is obtained by Fourier transforming the time-dependent dipole acceleration $d(t)$ of a model atom:

$$P_A(q\omega_1) = \left|\frac{1}{\sqrt{2\pi}}\int_0^T d(t)\,\mathrm{e}^{-\mathrm{i}q\omega_1 t}\,\mathrm{d}t\right|^2. \quad (4)$$

The time-dependent ionization probability is calculated by

$$P(t) = 1 - \sum_{\text{bound}} |\langle \varphi_n(x) \mid \psi(x,t)\rangle|^2 , \tag{5}$$

where the summation is over all the bound states $\varphi_n(x)$ when the laser field has been turned off.

To study the detailed spectral and temporal structures of HHG, we perform the time–frequency analysis by means of the wavelet transform [55, 56]

$$A(t_0,\omega_1) = \int d(t)\sqrt{\omega_1} W[\omega_1(t-t_0)]\,\mathrm{d}t, \tag{6}$$

where $W[\omega_1(t-t_0)]$ is the mother wavelet expressed as

$$W(x) = \left(\frac{1}{\sqrt{\tau}}\right) \mathrm{e}^{\mathrm{i}x}\,\mathrm{e}^{-x^2/2\tau^2}, \tag{7}$$

and $\tau = 30$ in our calculations.

By superposing several orders of harmonics, an attosecond pulse is generated and the temporal profile of the attosecond pulse is

$$I(t) = \left| \sum_q d_q\,\mathrm{e}^{\mathrm{i}q\omega_1 t} \right|^2 , \tag{8}$$

where $d_q = \int d(t)\,\mathrm{e}^{-\mathrm{i}q\omega_1 t}\,\mathrm{d}t$.

3. Results and Discussion

To verify our scheme, we first investigate the HHG process according to the classical three-step model. In this process, the motion of an electron under the combining force is described by the equation

$$\ddot{x}(t) = -E(t)\,. \tag{9}$$

Assuming the initial condition that the electron is ionized from the parent ion with zero velocity at t_i, we have

$$\dot{x}(t) = \int_{t_\mathrm{i}}^{t} -E(t)\,\mathrm{d}t \tag{10}$$

and

$$x(t) = \int_{t_\mathrm{i}}^{t} \dot{x}(t)\,\mathrm{d}t\,. \tag{11}$$

If the electron is ionized at t_i, the corresponding emission time t_e can be obtained by solving the equation

$$x(t_\mathrm{e}) = \int_{t_\mathrm{i}}^{t_\mathrm{e}} \dot{x}(t)\,\mathrm{d}t = 0\,. \tag{12}$$

The maximum kinetic energy E_k of the electron, which is ionized at t_i and returns to the parent ion at t_e, can be expressed as

$$E_\mathrm{k} = \frac{1}{2}\left[\int_{t_\mathrm{i}}^{t_\mathrm{e}} -E(t)\,\mathrm{d}t\right]^2 . \tag{13}$$

In our simulation, the laser intensity is far below the saturation intensity of the He^+ ion. According to the three-step model, the harmonic efficiency is mainly determined by the ionization rate, which is calculated by the ADK model [57]:

$$w(t) = \omega_\mathrm{p}\,|C_{n^*}|^2 \left(\frac{4\omega_\mathrm{p}}{\omega_\mathrm{t}}\right)^{2n^*-1} \exp\left(-\frac{4\omega_\mathrm{p}}{3\omega_\mathrm{t}}\right), \tag{14}$$

where

$$\omega_\mathrm{p} = \frac{I_\mathrm{p}}{\hbar}\,,\ \ \omega_\mathrm{t} = \frac{e\,|E(t)|}{\sqrt{2m_\mathrm{e}I_\mathrm{p}}}\,,\ \ n^* = Z\left(\frac{I_\mathrm{ph}}{I_\mathrm{p}}\right)^{1/2}, \tag{15}$$

$$|C_{n^*}|^2 = \frac{2^{2n^*}}{n^*\Gamma(n^*+1)\Gamma(n^*)}\,. \tag{16}$$

Z is the net resulting charge of the atom, I_ph is the ionization potential of the hydrogen atom, and e and m_e are electron charge and mass, respectively.

Figure 1a depicts the electric field of the two-colour field and the corresponding ionization rate. Figure 1b presents the corresponding dependence of the harmonic order on the ionization and emission times. Clearly, the electrons are mainly ionized near the peaks of the electric field and form four main peaks labelled as A_1, B_1, C_1, and D_1 on the returning energy map, respectively. The maximum harmonic order for B_1 is at the 572nd order due to the electrons ionized at $-0.53\,T_1$, and the maximum harmonic orders for C_1 and D_1 are the 255th and 253rd order, respectively, which are credited with the electrons ionized at $0.098\,T_1$ and $0.025\,T_1$. The contribution of A_1 to the HHG is inappreciable, so it can be ignored due to the low ionization rates of the corresponding electrons (i.e., electrons are ionized at about $-2.0\,T_1$ and $-1.05\,T_1$). Thus the harmonics above the 255th order are mainly contributed by B_1, which results in a 492 eV broadband XUV supercontinuum. However, in Figure 1a, the ionization rates of electrons ionized at about $-0.53\,T_1$, from which the supercontinuum originates, are much lower than that of electrons ionized at $0.098\,T_1$ and $0.025\,T_1$. Therefore, the harmonic

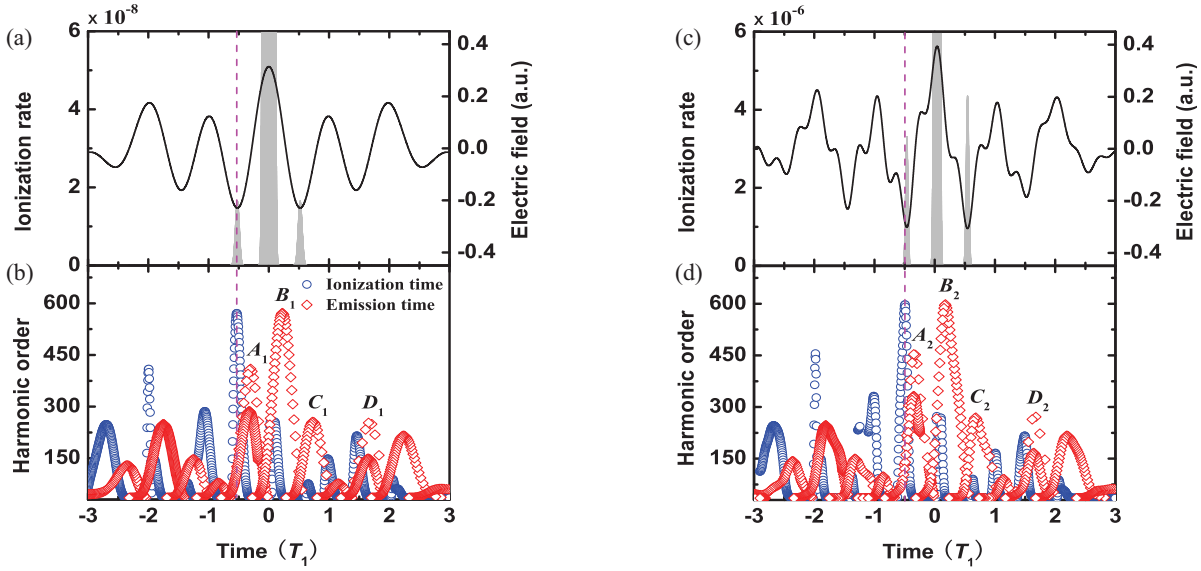

Fig. 1 (colour online). (a) Electric field of the two-colour field consisting of the 800 nm fundamental and 1600 nm subharmonic pulses and the corresponding ionization rate. (b) Dependence of the harmonic order on the ionization and emission times in the field shown in (a). (c) Electric field of the three-colour field synthesized by the two-colour field and 267 nm controlling pulse and the corresponding ionization rate. (d) Dependence of the harmonic order on the ionization and emission times in the field shown in (c).

yields of the supercontinuum are inefficient, leading to a double-plateau structure in the harmonic spectrum. For the supercontinuum, each order harmonic is generated only by two electron trajectories (so-called long and short trajectories); besides, the ionization rate with the short trajectory is comparable with that with the long one, so the interference between these two trajectories will lead to a strong modulated structure in the supercontinuum. The above results show that a supercontinuum with the bandwidth of 492 eV can be generated in the two-colour field, but the supercontinuum is inefficient and is attributed to the contribution of two electron trajectories, which are unfavourable for the generation of an isolated attosecond pulse.

We can control the electron trajectories for HHG in the two-colour field and enhance the corresponding ionization rate by adding a weak 267 nm controlling pulse. In order to substantiate this fact, we perform the classical trajectory simulation of the electrons and calculate the corresponding ionization rate in the three-colour field. The results are shown in Figure 1c and d. As shown in Figure 1d, there are still four major peaks labelled as A_2, B_2, C_2, and D_2 on the returning energy map. The contribution of A_2 to the HHG is negligible due to its low ionization rate, which is similar to that in the two-colour field. Thus the HHG emission mainly originates from B_2, C_2, and D_2, which are caused by the electrons ionized at $-0.49\,T_1$, $0.1\,T_1$, and $0.032\,T_1$, respectively. The maximum order harmonic of B_2 reaches 598, whereas that of D_2 reaches 273. C_2 contributes to many orders of harmonics up to 267th. Compared with the two-colour case, since the highest order of the harmonics is higher, the spectral cutoff for the case is extended. Moreover, the energy difference between B_2 and D_2 is 504 eV, thus a broad supercontinuum covering a 504 eV bandwidth is generated and is superior to that for the two-colour case. Further, with the introduction of the 267 nm controlling pulse, the ionization rates of electrons contributing to the harmonic generation are extremely different. As shown by a grey filled curve in Figure 1c, the corresponding ionization rates of B_2, C_2, and D_2 are at least two orders of magnitude higher than those of B_1, C_1, and D_1 in Figure 1a, implying the efficient enhancement of the harmonic yields in the three-colour field. It is worthwhile to note that for the supercontinuum there is mainly a long trajectory and a short trajectory contributing to the same harmonic order with the same return energy. Electrons with the long trajectory are mainly ionized from $-0.62\,T_1$ to $-0.49\,T_1$,

and electrons with the short trajectory are mainly ionized from $-0.49\,T_1$ to $-0.33\,T_1$, however, the ionization rate for the short trajectory is much higher than that for the long trajectory. In addition, electrons with the long trajectory travel a longer time in the continuous state, which results in a lower harmonic efficiency due to the quantum diffusion. Consequently, the harmonic efficiency for the short trajectory is much higher than that for the long trajectory, i.e., the short trajectory is selected effectively to contribute to the supercontinuum, and the harmonic spectrum of the supercontinuum is much smoother, which is contributed by the large reduction of the interference of the long and short trajectories. Considering all the results above, we can conclude that a high-efficiency broadband XUV supercontinuum with a bandwidth of 504 eV and the selection of the single electron trajectory can be achieved by adding the 267 nm controlling pulse, which is highly likely to support the generation of an efficient isolated ultrashort attosecond pulse.

To confirm the above classical results, we investigate the harmonic spectrum using the full quantum calculation. All the parameters are the same as those in Figure 1. In Figure 2a, we show the harmonic spectra of the He^+ ion in the two-colour field (dashed blue line) and in the three-colour field (dotted red line), respectively. For comparison, the harmonic spectrum in the 800 nm fundamental pulse alone is also given. As shown by the solid black line in Figure 2a, the spectrum cutoff is only at the 284th order, and the spectral structure above the 260th order is continuous. Thus the supercontinuum with a bandwidth of only 37 eV is generated near the cutoff region. Such a narrow spectrum is difficult to produce attosecond pulses with short duration. For the two-colour case, the harmonic spectrum presents an apparent two-plateau structure, and the spectral cutoff is significantly extended to the 597th order. The harmonics from the 280th order to the cutoff become continuous, which results in a 492 eV supercontinuum (i.e., the whole second plateau). Compared with the case of the single 800 nm fundamental pulse, both the harmonic cutoff and the supercontinuum width are dramatically enlarged. Therefore, the major role of the 1600 nm control pulse in the two-colour field is to extend the spectral cutoff and generate a broadband supercontinuum. However, on the one hand, the supercontinuum has a low conversion efficiency, which is attributable to the low ionization rates of the corresponding electrons; on the other hand, the supercontinuum shows a large modulation structure, which is due to the interference of the long and the short paths. Thereby, these properties for the supercontinuum in the two-colour field are unfavourable for generating an intense single attosecond pulse. With the addition of the 267 nm controlling pulse, the overall harmonic spectrum is uplifted and the spectral structure is similar to the two-colour case, as displayed by the dotted red line in Figure 2a. The spectrum cutoff is at about the 619th order and the harmonics above the 294th order become regular and continuous, corresponding to a supercontinuum with a bandwidth of 504 eV. The modulation in the supercontinuum is much reduced, implying a single quantum path is selected. In addition, the harmonic intensity is effectively enhanced by $1\sim2$ orders of magnitude compared with the two-colour case. Such harmonic enhancement can be well understood by the time-dependent ionization probabilities shown in Figure 2b, where the ionization probabilities of electrons in the three-colour field (dashed red line) is much larger than that in the two-colour field (dotted blue line). The underlying reason lies in that the 267 nm laser pulse can promote the multi-photon resonant transitions from the $1s$ to the $2s$ or $2p$ state. The electrons populated in the states are easily ionized by the driving field owing to the low binding energy. Thus the ionization yields are increased significantly. As a result, the conversion efficiency of the harmonic spectrum is improved dramatically compared with the two-colour case. Therefore, by adding the 267 nm controlling pulse to the two-colour field, a high-efficiency broadband supercontinuum and the selection of the single quantum path can be achieved.

A deeper insight is obtained by investigating the emission times of the harmonics in terms of the time–frequency analysis method. For comparison, the time–frequency distribution of the HHG spectrum in the two-colour field is also given. As shown in Figure 3a, there are four main peaks (marked as A_1, B_1, C_1, and D_1) with the maximum harmonic orders of 409, 597, 280, and 278 contributing to the harmonic generation. Among these four peaks, the intensity of A_1 is much weaker than those of the other three peaks, so its contribution to the HHG can be ignored. Thus the harmonics higher than the 280th order are mainly contributed by B_1, forming a 492 eV supercontinuum (i.e., the harmonics in the second plateau). The intensity of B_1 is much lower than those of C_1 and D_1, which is the rea-

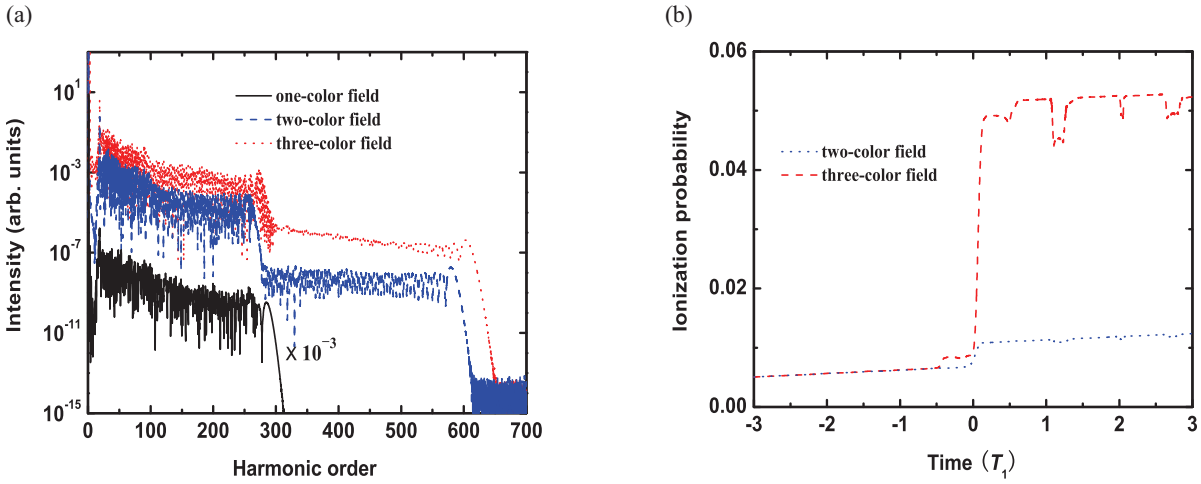

Fig. 2 (colour online). (a) Harmonic spectra of the He^+ ion in the 800 nm fundamental pulse alone (solid black line), in the two-colour field (dashed blue line), and in three-colour field (dotted red line), respectively. Note that the harmonic intensity for the single 800 nm fundamental pulse is multiplied by a factor of 10^{-3} for the sake of clarity. (b) The time-dependence ionization probabilities in the two-colour field (dotted blue line) and in the three-colour field (dashed red line), respectively.

son for the two-plateau structure and simultaneously implies that the harmonic yields of the supercontinuum is inefficient. For the supercontinuum, there are two emission times for the same harmonic in the half-cycle of the driving pulse, which corresponds to the long and short quantum paths (the left branch: the short quantum path; the right branch: the long quantum path). Since the intensities for the two quantum paths are almost comparable, the interference between them gives rise to a distinct modulation in the supercontinuum, as shown by the dashed blue line in Figure 2a. Figure 3b is the time–frequency distribution of HHG in the three-colour field, which shows that there are still four major peaks (marked as A_2, B_2, C_2, and D_2) with the maximum harmonic orders of 453, 619, 290, and 294 in the time–frequency distribution. The contribution of A_2 to the HHG can be ignored due to the low harmonic yields. Then the bandwidth of the supercontinuum is directly determined by the energy difference between B_2 and D_2, which leads to the generation of a 504 eV supercontinuum. In addition, the two branches of B_2 are much brighter than those of B_1 in Figure 3a, implying the efficient enhancement of the supercontinuum. For the peak B_2, the left branch is much more dominant than the right one, which is responsible for a broadband smooth supercontinuum in the second plateau and synchronously indicates that the short quantum path is selected to dominate the supercontinuum generation. All of these results are consistent with those with the classical approaches.

Through the above analysis, a high-efficiency broadband supercontinuum and the selection of a single quantum path can be achieved by the three-colour field, which can be used to generate an intense isolated ultrashort attosecond pulse. In order to check this viewpoint, we investigate the attosecond pulse generation in the three-colour field. For comparison, the attosecond pulse generated in the two-colour field is also given. As shown in Figure 4a, by superposing 80 order harmonics from 300 to 380, two radiation pulses with durations of 35.5 as and 33.6 as are generated in each optical cycle. This is because there are two quantum paths with different emission times contributing to the same harmonic shown in Figure 3a. Since the plateau harmonics are not emitted at the same time, the superposition of several order harmonics will result in two radiation pulses. Such a chain of attosecond pulses is very difficult to use in the pump-probe experiment or the measurement of ultrafast dynamic processes. Figure 4b shows the attosecond pulse generation from the supercontinuum in the three-colour field. By applying a frequency window with a bandwidth of 140 eV to the supercontinuum, an isolated ultrashort attosecond pulse is directly generated without phase compensation. As the frequency window is moved along the harmonic order axis, the duration of the attosecond pulse is 30 as

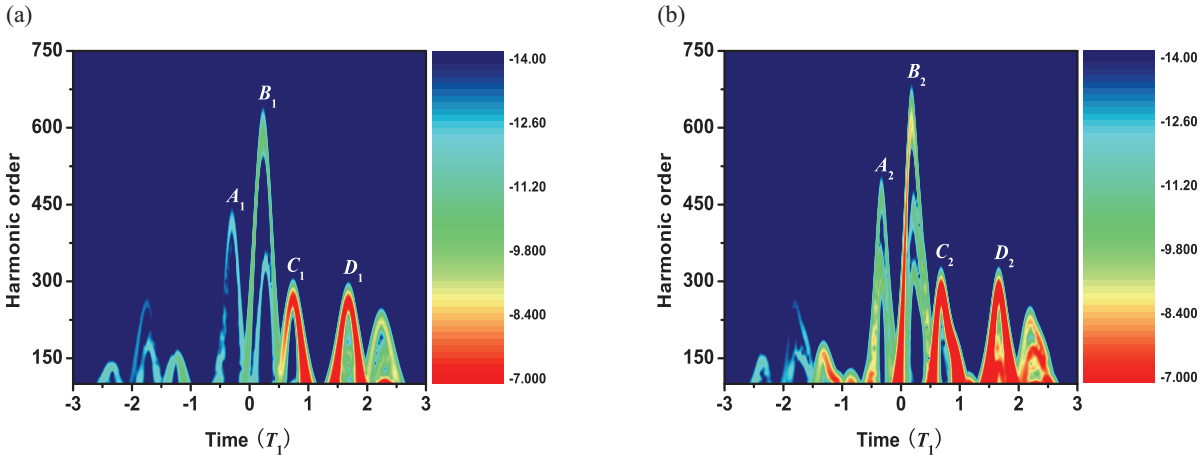

Fig. 3 (colour online). (a) Time-frequency distribution of the HHG spectrum corresponding to the dashed blue line in Figure 2a. (b) Time-frequency distribution of the HHG spectrum corresponding to the dotted red line in Figure 2a.

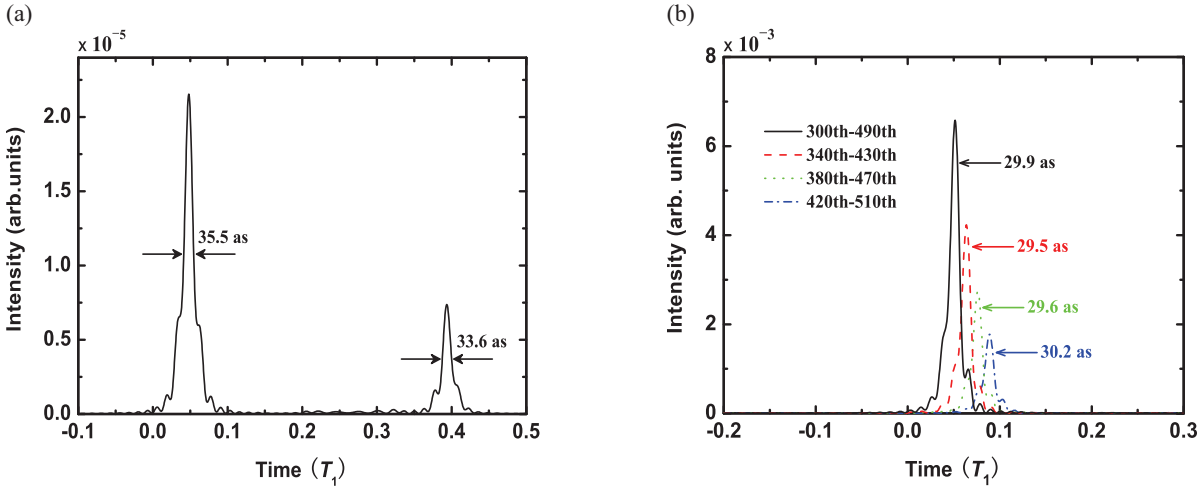

Fig. 4 (colour online). (a) Temporal profiles of the attosecond pulses by superposing the harmonics from 300th to 380th in the two-colour field. (b) Temporal profiles of the attosecond pulses by superposing 90 order harmonics in different spectral regions in the three-colour field.

and does not change. This reflects that the duration of the generated attosecond pulse is insensitive to the position of the frequency window. In addition, though the intensity of the generated attosecond pulse decreases with increasing the central frequency, which is caused by the decrease of the harmonic efficiency as the harmonic order increases, the intensity of each pulse is several times higher than that in the two-colour field (about two orders of magnitude higher). Our calculations also show that (not presented here) the single attosecond pulse presented in Figure 4b can be obtained by superposing an arbitrary 90-order harmonics in the supercontinuum from 294th to 520th order, which provides a convenient method to obtain an isolated 30 as pulse with a stable pulse duration in experiment.

In our simulation, we find that the extension of the harmonic cutoff and the enhancement of the supercontinuum as well as an isolated 30 as pulse generation can be achieved for the time delay (τ_{delay}) varying from $-0.035\ T_1$ to $-0.075\ T_1$ and $0.26\ T_1$ to $0.30\ T_1$. To verify the facts, we first investigate the harmonic spectra generated in the three-colour field with six different

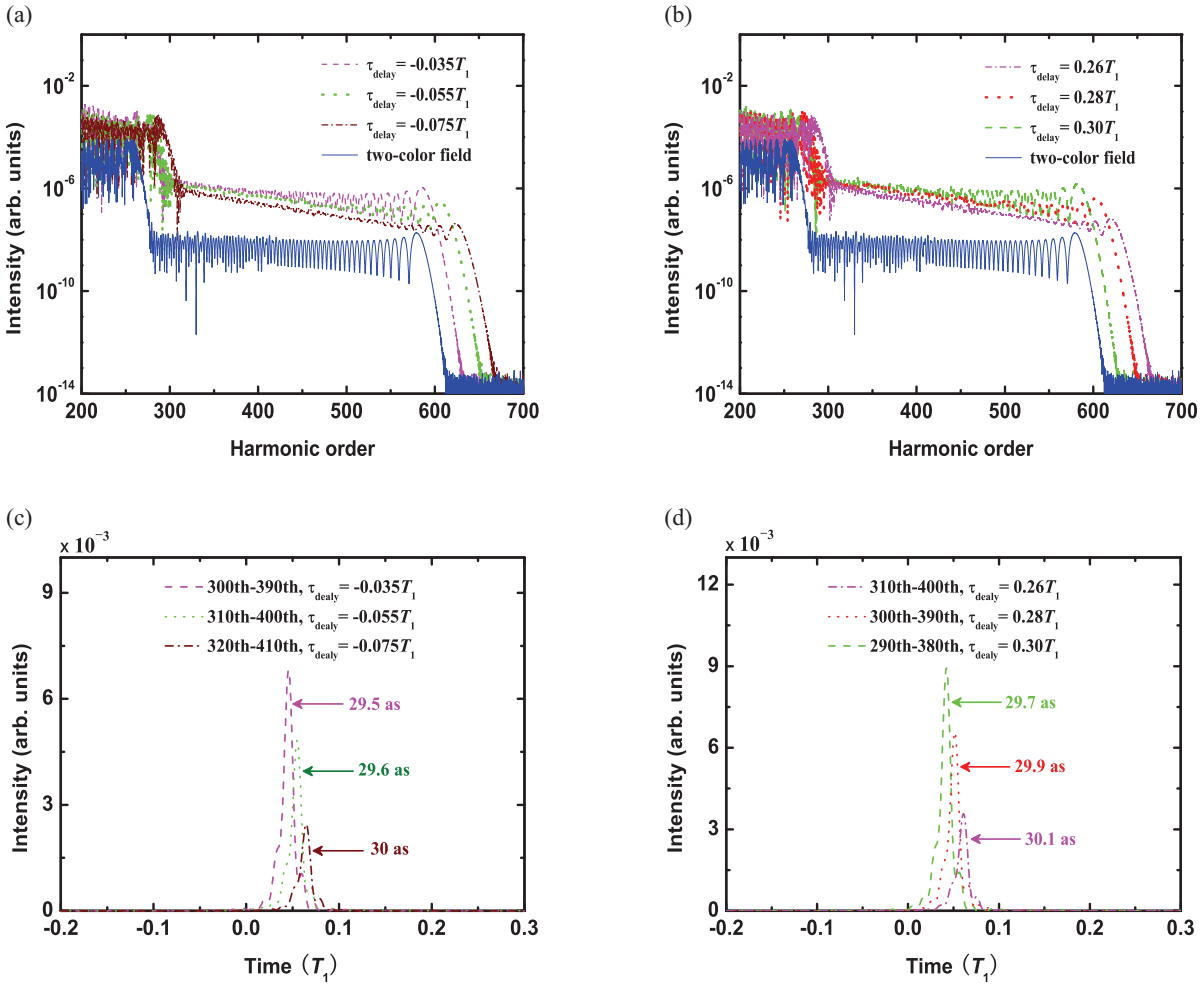

Fig. 5 (colour online). (a) High energy part of the harmonic spectra with three different time delays: dashed line, $\tau_{\text{delay}} = -0.035\,T_1$; dotted line, $\tau_{\text{delay}} = -0.055\,T_1$; dot-dashed line, $\tau_{\text{delay}} = -0.075\,T_1$. (b) The same as (a) but for the other three time delays: dot-dashed line, $\tau_{\text{delay}} = 0.26\,T_1$; dotted line, $\tau_{\text{delay}} = 0.28\,T_1$; dashed line, $\tau_{\text{delay}} = 0.30\,T_1$. (c) and (d) Temporal profiles of the attosecond pulses for the cases of six corresponding time delays.

time delays. The results are shown in Figure 5a and b. For comparison, the harmonic spectrum generated by the two-colour field is also given. Clearly, as the time delay changes from $-0.035\,T_1$ to $-0.075\,T_1$, the spectral cutoff increases from 602nd to 634th order, as the time delay changes from $0.26\,T_1$ to $028\,T_1$, the spectral cutoff decreases from 630th to 599th order; but each of the spectral cutoffs for these six cases is larger than that in the two-colour field. (Note that the spectrum cutoff for the two-colour case is at the 597th order harmonic.) In addition, from Figure 5a and b, the harmonic yields of the supercontinuum for the case of each time delay are higher than that of the harmonics at the same orders in the two-colour field and the supercontinuum covers a very wide frequency range, implying that the broadband supercontinuum with high efficiency can be obtained for the cases of different time delays. Next, we present the generation of the isolated attosecond pulses for the cases of six corresponding time delays, which are shown in Figure 5c and d. As seen from these two figures, for the case of each time delay, a pure isolated attosecond pulse with the duration of about 30 as is directly produced by superposing 90-order harmonics in the supercontinuum and its intensity is two or-

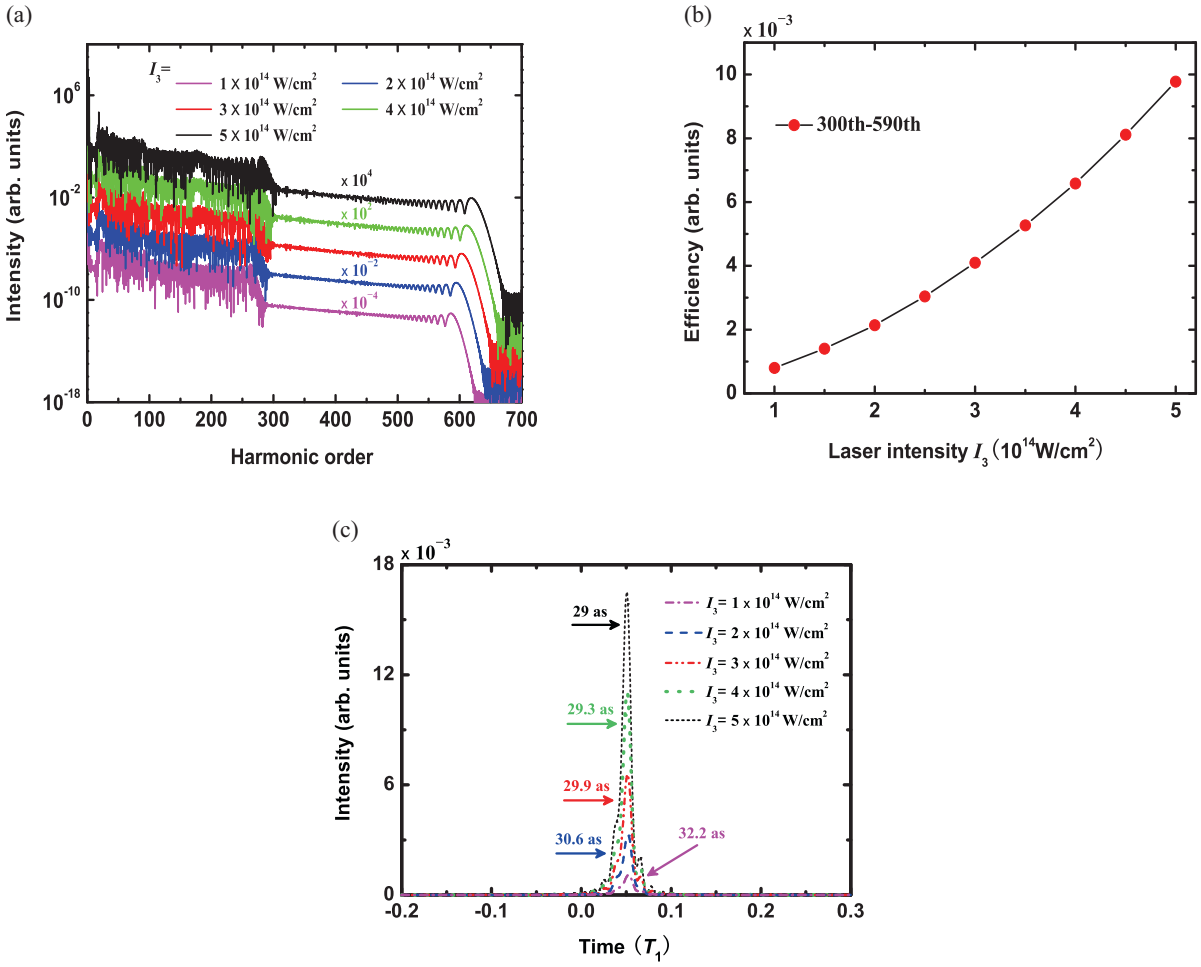

Fig. 6 (colour online). (a) Harmonic spectra with five different intensities of the 267 nm controlling pulse. For the purpose of clarity, the harmonic intensities for $1 \cdot 10^{14}$, $2 \cdot 10^{14}$, $4 \cdot 10^{14}$, and $5 \cdot 10^{14}$ W/cm^2 are multiplied by factors of 10^{-4}, 10^{-2}, 10^2, and 10^4, respectively. (b) The emitted efficiency of the supercontinuum from 300th to 590th order as a function of I_3. (c) Temporal profiles of the attosecond pulses generated by superposing the harmonics from 300th to 390th for the cases of five corresponding intensities of the 267 nm controlling pulse.

ders of magnitude higher than that in the two-colour field. This implies that an intense isolated 30 as pulse can be generated in a wide range of the time delay of the 267 nm controlling pulse with respect to the driving pulse, which facilitates the experimental implement of the strong isolated ultrashort attosecond pulse generation.

We also investigate the influence of the intensity of the 267 nm controlling pulse (I_3) on the harmonic spectrum and isolated attosecond pulse generation. Other laser parameters are the same as those in Figure 1. Figure 6a presents the harmonic spectra with five different intensities of the 267 nm controlling pulse: $1 \cdot 10^{14}$, $2 \cdot 10^{14}$, $3 \cdot 10^{14}$, $4 \cdot 10^{14}$, and $5 \cdot 10^{14}$ W/cm^2, respectively. Since the harmonics in the plateau region for five curves have some overlaps, so we shift four curves for the purpose of clarity so that the harmonic signals of $1 \cdot 10^{14}$, $2 \cdot 10^{14}$, $4 \cdot 10^{14}$, and $5 \cdot 10^{14}$ W/cm^2 are scaled. As seen from this figure, the harmonic spectra for these five cases present a prominent two-plateau structure with two cutoffs, and the harmonics in the second plateau are regular and continuous, from which the supercontinuum originates. With increasing the intensity of the controlling pulse, the

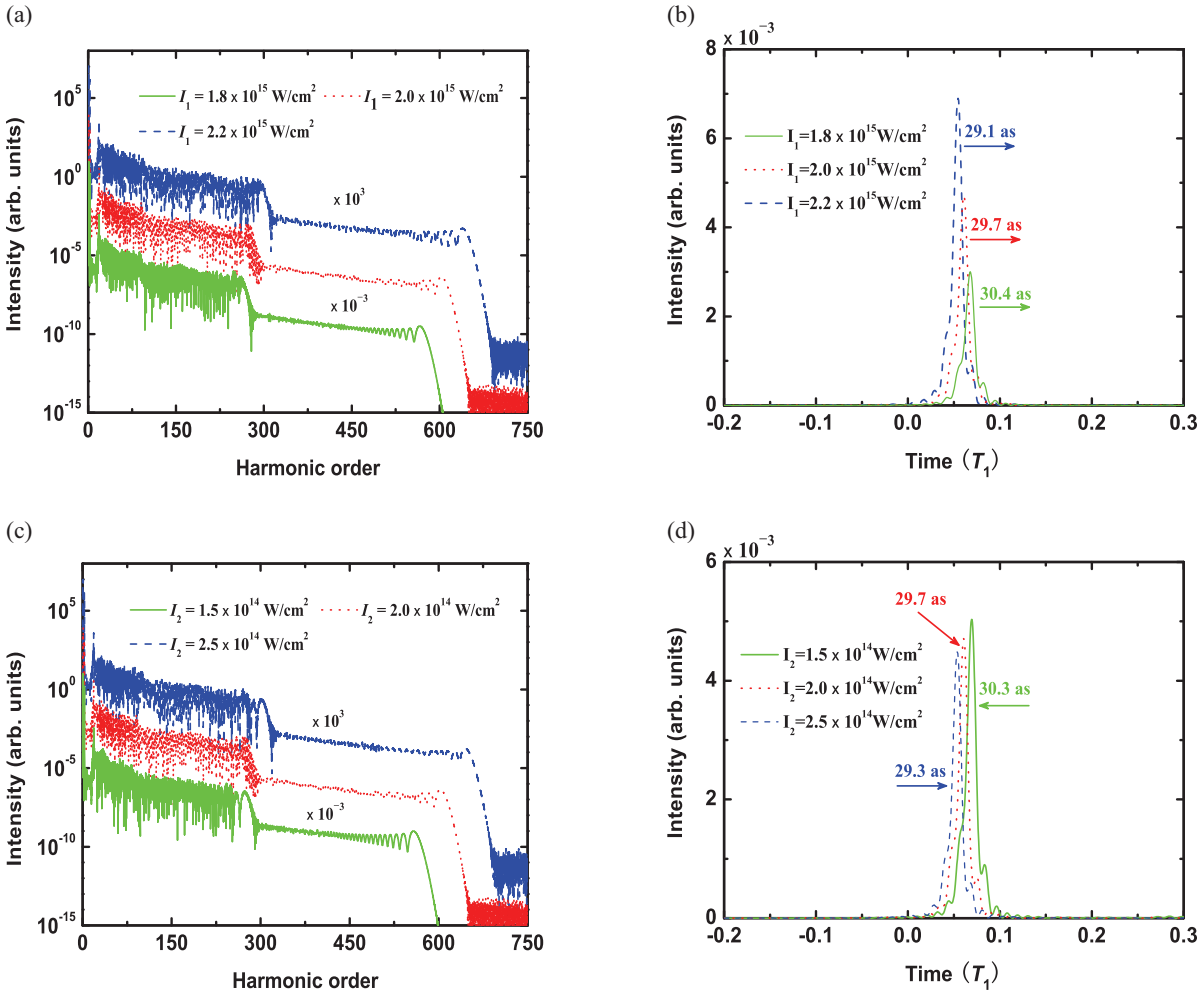

Fig. 7 (colour online). (a) Harmonic spectra with three different intensities of the 800 nm fundamental pulse. For the purpose of clarity, the harmonic intensities for $1.8 \cdot 10^{15}$ and $2.2 \cdot 10^{15}$ W/cm^2 are multiplied by factors of 10^{-3} and 10^3, respectively. (b) Temporal profiles of the attosecond pulses generated by superposing the harmonics from 330th to 420th with three different intensities of the 800 nm fundamental pulse. (c) and (d) The same as (a) and (b) but for the 1600 nm subharmonic pulse.

start point and the end point of the continuum spectrum increase, but the change of the end point is larger than that of the start point, and then the bandwidth of the supercontinuum is enlarged. In addition, the increase of the intensity of the controlling pulse directly leads to the extension of the spectral cutoff. From Figure 6a, one can see clearly that, with the increasing of the intensity of the controlling pulse, the modulation of the supercontinum becomes strong but is not immediately obvious, implying the broadband smooth supercontinuum can be generated by using a stronger controlling pulse. The emitted efficiency of the supercontinuum is also associated with the intensity of the controlling pulse. When the intensity of the controlling pulse is in the range of $1 \cdot 10^{14}$ W/cm$^2 \sim 5 \cdot 10^{14}$ W/cm^2, the continuum spectrum contains the harmonics from 300th to 590th order. Therefore, we investigate the efficiency of these harmonics with different intensities of the 267 nm controlling pulse. Figure 6b shows the emitted efficiency of the supercontinuum as a function of I_3. Note that the emitted efficiency of the supercontinuum can be obtained by summing the harmonic

intensities from 300th to 590th. The calculated result shows that the emitted efficiency increases nearly linearly as the intensity of the control pulse increases, indicating the harmonic yields of the supercontinuum can be enhanced by increasing the intensity of the controlling pulse. Moreover, under the condition of $I_3 \geq 10^{14}\,\mathrm{W/cm^2}$, the emitted efficiency of the supercontinuum from 300th to 590th order in the three-colour field is at least an order of magnitude higher than that of the harmonics at the same orders in the two-colour field, then the yields of this supercontinuum are much more efficient than that in the two-colour field. Further, we also consider the isolated attosecond pulse generation for the cases of five corresponding intensities of the 267 nm controlling pulse, which is shown in Figure 6c. Here the harmonics from 300th to 390th order are selected to synthesize an isolated attosecond pulse. The corresponding bandwidth is about 140 eV. As shown in Figure 6c, in all the cases, pure isolated attosecond pulses can be obtained and the emission times and pulse durations of these five isolated attosecond pulses are little changed; besides, when the intensity of the controlling pulse increases, the intensity of the isolated attosecond pulse increases. These results implies that the spectral cutoff and the width and the harmonic yields of the supercontinuum as well as the intensity of the isolated 30 as pulse can be further enhanced by using a stronger controlling pulse. For the cases of other time delays mentioned in Figure 5, similar results can be obtained.

Finally, we investigate the influences of the intensities of the 800 nm fundamental and 1600 nm subharmonic pulses on the supercontinuum and isolated attosecond pulse generation in the three-colour field. Other parameters are the same as those in Figure 1. Figure 7a presents the harmonic spectra with three different intensities of the 800 nm fundamental pulse: $1.8 \cdot 10^{15}$, $2.0 \cdot 10^{15}$, and $2.2 \cdot 10^{15}\,\mathrm{W/cm^2}$, respectively. As shown in this figure, as the intensity of the fundamental pulse increases, the first cutoff and the second one of the harmonic spectrum increase, whereas the increase of the second cutoff is greater than that of the first one. Thus the frequency difference between two cutoffs is enlarged, which also lead to the widening of the supercontinuum. From Figure 7a, it can be seen that though some modulations appear clearly in the supercontinuum with the increase of the intensity of the fundamental pulse, this has little effect on the generation of an isolated 30 as pulse as shown in Figure 7b. The three attosecond pulses in Figure 7b correspond to three different intensities of the fundamental pulse. Comparing the three curves in Figure 7b, the intensities of the isolated attosecond pulse are increased with increasing the intensity of the fundamental laser, and the emission times and pulse durations of these three isolated attosecond pulses are changed slightly. The same is true if the intensity of the subharmonic pulse is increased, as shown in Figure 7c. Just the spectral cutoff and the bandwidth of the supercontinuum are greatly extended in comparison with that in Figure 7a. In addition, one can see from Figure 7c that the supercontinuum becomes smoother for the relatively large laser intensity, which implies the interference of the long and short paths can be largely eliminated by enhancing the intensity of the subharmonic pulse. Figure 7d presents the temporal profiles of the attosecond pulses generated by superposing the harmonics from 330th to 420th for three different intensities of the 1600 nm subharmonic pulse, which show that the emission times and the intensities of the attosecond pulses as well as the durations of the attosecond pulses change slightly. Therefore, regular attosecond pulses with durations of about 30 as can be obtained with the three different intensities for the subharmonic laser. These results show that the spectral cutoff and the supercontinuum width can be extended by properly enhancing the intensity of either the fundamental pulse or the subharmonic pulse, and then single isolated 30 as pulses can be generated directly.

4. Conclusions

In summary, we theoretically present a multi-cycle three-colour field scheme to generate an intense isolated ultratshort attosecond pulse. It is shown that this method can not only enhance the spectral cutoff and the yields of the harmonic spectrum, but also realise the selection of the single quantum path, and then the supercontinuum with high efficiency and less modulated structure is generated. Since the supercontinuum covers an extremely broad bandwidth and mainly originates from the contribution of the single short path, an intense isolated ultrashort 30 as pulse is directly obtained without phase compensation. In addition, we also investigate the influence of the time delay of the 267 nm controlling pulse on the supercontinuum and isolated attosecond pulse generation. The result shows that the broadband supercontinuum

with high efficiency and intense isolated attosecond pulses with durations of about 30 as can be generated in a wide time delay range. By using a stronger 267 nm controlling pulse, the harmonic cutoff and the width and yields of the supercontinuum can be further enhanced, and then the generated isolated 30 as pulse is much more efficient. Moreover, the effects of the intensities of the fundamental and subharmonic fields on the supercontinuum and isolated attosecond pulse generation are also investigated. The numerical results show that the extension of the spectral cutoff and the supcontinuum and the production of isolated 30 as pulses can be achieved. These properties are very beneficial to the experimental implement for the generation of isolated ultrashort attosecond pulses with stable pulse durations. Finally, we would like to point out the feasibility of the scheme. Presently, a 10 fs, 800 nm laser pulse is available in a good few laboratories, and a 24 fs, 1600 nm subharmonic pulse can be generated by optical parametric amplifier (OPA), besides, a 10 fs, 267 nm controlling pulse can be obtained from a beta-barium-borate (BBO) crystal. Therefore, the scheme presented here appears feasible for an experimental demonstration in the near future. To sum up, the advantage of our scheme lies in producing an ultrabroad supercontinuum and maintaining a high conversion efficiency, which is beneficial for generating an intense isolated ultrashort attosecond pulse.

Acknowledgement

This work was supported by the Science Foundation of Baoji University of Arts and Sciences, China (Grant No. ZK11061) and the Education Committee Natural Science Foundation of Shaanxi Province, China (Grant No. 2013JK0637).

[1] P. M. Paul, E. S. Toma, P. Breger, G. Mullot, F. Augé, P. Balcou, H. G. Muller, and P. Agostini, Science **292**, 1689 (2001).
[2] Y. Mairesse, A. de Bohan, L. J. Frasinski, H. Merdji, L. C. Dinu, P. Monchicourt, P. Breger, M. Kovačv, R. Taïeb, B. Carré, H. G. Muller, P. Agostini, and P. Salières, Science **302**, 1540 (2003).
[3] M. Drescher, M. Hentschel, R. Kienberger, M. Uiberacker, V. Yakovelv, A. Scrinzi, T. Westerwalbesloh, U. Kleineberg, U. Heinzmann, and F. Krausz, Nature **419**, 803 (2002).
[4] R. Kienberger, E. Goulielmakis, M. Uiberacker, A. Baltuska, V. Yakovlev, F. Bammer, A. Scrinzi, T. Westerwalbesloh, U. Kleineberg, U. Heinzmann, M. Drescher, and F. Krausz, Nature **427**, 817 (2004).
[5] P. B. Corkum, Phys. Rev. Lett. **71**, 1994 (1993).
[6] P. Antoine, A. L'Huillier, and M. Lewenstein, Phys. Rev. Lett. **77**, 1234 (1996).
[7] I. P. Christov, M. M. Murnane, and H. C. Kapteyn, Phys. Rev. Lett. **78**, 1251 (1997).
[8] A. Baltuska, T. Udem, M. Uiberacker, M. Hentschel, E. Goulielmakis, C. Gohle, R. Holzwarth, V. S. Yakovlev, A. Scrinzi, T. W. Hänsch, and F. Krausz, Nature **421**, 611 (2003).
[9] E. Goulielmakis, M. Schultze, M. Hofstetter, V. S. Yakovlev, J. Gagnon, M. Uiberacker, A. L. Aquila, E. M. Gullikson, D. T. Attwood, R. Kienberger, F. Krausz, U. Kleineberg, Science **320**, 1614 (2008).
[10] G. Sansone, E. Benedetti, F. Calegari, C. Vozzi, L. Avaldi, R. Flammini, L. Poletto, P. Villoresi, C. Altucci, R. Velotta, S. Stagira, S. D. Silvestri, and M. Nisoli, Science **314**, 443 (2006).
[11] P. F. Lan, P. X. Lu, W. Cao, Y. H. Li, and X. L. Wang, Phys. Rev. A **76**, 051801 (2007).
[12] J. J. Carrera and S. I. Chu, Phys. Rev. A **75**, 033807 (2007).
[13] Z. H. Chang, Phys. Rev. A **76**, 051403 (2007).
[14] H. Mashiko, S. Gilbertson, C. Li, S. D. Khan, M. M. Shakya, E. Moon, and Z. H. Chang, Phys. Rev. Lett. **100**, 103906 (2008).
[15] X. M. Feng, S. Gilberston, H. Mashiko, H. Wang, S. D. Khan, M. Chini, Y. Wu, K. Zhao, and Z. H. Chang, Phys. Rev. Lett. **103**, 183901 (2009).
[16] C. Altucci, J. W. G. Tisch, and R. Velotta, J. Mod. Optic. **58**, 1585 (2011).
[17] C. Altucci, R. Velotta, V. Tosa, P. Villoresi, F. Frassetto, L. Poletto, C. Vozzi, F. Calegari, M. Negro, S. De Silvestri, and S. Stagira, Opt. Lett. **35**, 2798 (2010).
[18] K. Zhao, Q. Zhang, M. Chini, Y. Wu, X. W. Wang, and Z. H. Chang, Opt. Lett. **37**, 3891 (2012).
[19] Z. N. Zeng, Y. Cheng, X. H. Song, R. X. Li, and Z. Z. Xu, Phys. Rev. Lett. **98**, 203901 (2007).
[20] P. F. Lan, P. X. Lu, W. Cao, Y. H. Li, and X. L. Wang, Phys. Rev. A **76**, 011402 (2007).
[21] W. Cao, P. X. Lu, P. F. Lan, W. Y. Hong, and X. L. Wang, J. Phys. B **40**, 869 (2007).
[22] F. I. Gauthey, C. H. Keitel, P. L. Knight, and A. Maquet, Phys. Rev. A **52**, 525 (1995).
[23] B. B. Wang, T. W. Cheng, X. F. Li, and P. M. Fu, Phys. Rev. A **72**, 063412 (2005).

[24] Z. Zhai, R. F. Yu, X. S. Liu, and Y. J. Yang, Phys. Rev. A **78**, 041402 (2008).
[25] J. G. Chen, Y. J. Yang, S. L. Zeng, and H. Q. Liang, Phys. Rev. A **83**, 023401 (2011).
[26] W. Y. Hong, Q. B. Zhang, X. S. Zhu, and P. X. Lu, Opt. Express **19**, 4728 (2011).
[27] L. Q. Feng and T. S. Chu, Phys. Lett. A **376**, 1523 (2012).
[28] J. H. Luo, Y. Li, Z. Wang, Q. B. Zhang, P. F. Lan, and P. X. Lu, J. Opt. Soc. Am. B **30**, 2469 (2013).
[29] G. T. Zhang, Mol. Phys. **111**, 3117 (2013).
[30] S. F. Zhao, X. X. Zhou, P. C. Li, and Z. J. Chen, Phys. Rev. A **78**, 063404 (2008).
[31] J. H. Luo, Y. Li, Z. Wang, L. X. He, Q. B. Zhang, P. F. Lan, and P. X. Lu, Phys. Rev. A **89**, 023405 (2014).
[32] L. Q. Feng and T. S. Chu, IE. E. E. J. Quantum Elect. **48**, 1462 (2012).
[33] C. M. Kim, I. J. Kim, and C. H. Nam, Phys. Rev. A **72**, 033817 (2005).
[34] M. B. Gaarde, K. J. Schafer, A. Heinrich, J. Biegert, and U. Keller, Phys. Rev. A **72**, 013411 (2005).
[35] K. J. Schafer, M. B. Gaarde, A. Heinrich, J. Biegert, and U. Keller, Phys. Rev. Lett. **92**, 023003 (2004).
[36] M. Bellini, C. Lynga, A. Tozzi, M. B. Gaarde, T. W. Hänsch, A. L'Huillier, and C. G. Wahlström, Phys. Rev. Lett. **81**, 297 (1998).
[37] P. Antoine, A. L'Huillier, and M. Lewenstein, Phys. Rev. Lett. **77**, 1234 (1996).
[38] P. F. Lan, P. X. Lu, Q. G. Li, F. Li, W. Y. Hong, and Q. B. Zhang, Phys. Rev. A **79**, 043413 (2009).
[39] P. F. Lan, P. X. Lu, F. Li, Q. G. Li, W. Y. Hong, Q. B. Zhang, Z. Y. Yang, and X. B. Wang, Opt. Express **16**, 17542 (2008).
[40] M. B. Gaarde, J. L. Tate, and K. J. Schafer, J. Phys. B **41**, 132001 (2008).
[41] L. E. Chipperfield, J. S. Robinson, J. W. G. Tisch, and J. P. Marangos, Phys. Rev. Lett. **102**, 063003 (2009).
[42] M. Negro, C. Vozzi, K. Kovacs, C. Altucci, R. Velotta, F. Frassetto, L. Poletto, P. Villoresi, S. De Silvestri, V. Tosa, and S. Stagira, Laser Phys. Lett. **8**, 875 (2011).
[43] T. Balčiíĺśnas, S. Haessler, G. Y. Fan, G. Andriukaitis, A. Pugžlys, A. Baltuška, A. Zaïr, R. Squibb, L. Chipperfield, L. Frasinski, J. W. G. Tisch, and J. Marangos, EPJ Web of Conferences **41**, 01017 (2013).
[44] C. Jin, G. L. Wang, H. Wei, A. T. Le, and C. D. Lin, Nat. Commun. **5**, 4003 (2014).
[45] H. C. Bandulet, D. Comtois, E. Bisson, A. Fleischer, H. Pĺępin, J. C. Kieffer, P. B. Corkum, and D. M. Villeneuve, Phys. Rev. A **81**, 013803 (2010).
[46] R. F. Lu, H. X. He, Y. H. Guo, and K. L. Han, J. Phys. B **42**, 225601 (2009).
[47] L. Q. Feng and T. S. Chu, Phys. Lett. A **375**, 3641 (2011).
[48] P. C. Li, I. L. Liu, and S. I. Chu, Opt. Express **19**, 23857 (2011).
[49] H. N. Du and X. Y. Miao, Spectrosc. Lett. **45**, 556 (2012).
[50] H. C. Du, H. Q. Wang, and B. T. Hu, Phys. Rev. A **81**, 063813 (2010).
[51] H. C. Du, Y. Z. Wen, X. S. Wang, and B. T. Hu, Opt. Express **21**, 21337 (2013).
[52] L. X. He, Y. Li, Q. B. Zhang, and P. X. Lu, Opt. Express **21**, 2683 (2013).
[53] M. D. Feit, J. A. Fleck Jr, and A. Steiger, J. Comput. Phys. **47**, 412 (1982).
[54] K. Burnett, V. C. Reed, J. Cooper, and P. L. Knight, Phys. Rev. A **45**, 3347 (1992).
[55] P. Antoine, B. Piraux, and A. Maquet, Phys. Rev. A **51**, R1750 (1995).
[56] J. J. Carrera, X. M. Tong, and S. I. Chu, Phys. Rev. A **74**, 023404 (2006).
[57] M. V. Ammosov, N. B. Delone, and V. P. Krainov, Sov. Phys. JETP **64**, 1191 (1986).